1   *Article*

2 Fracture Failure Mechanisms of Long Single PA6
3 Fibers

4   **Huiling Ding [1,2],   Yongzhen Zhang [3,*] and Zhitao He [2,]**

5   [1] *School of Mechanical Engineering Northwestern Polytechnical University，Xi'an 710000，China*;
6   ding-huiling@163.com (H. D.)
7   [2] *School o of Agricultural Equipment Engineering Henan University of Science and Technology，Luoyang 471023 China*;
8   hezt79@163.com (Z.H.)
9   [3] *School of Materials Science and Engineering Henan University of Science and Technology, Luoyang 471023 China*;
10   ***** Correspondence: yzzhang@haust.edu.cn (Y. Z.)Tel.: +86‒379‒64231003; Fax: +86‒379‒64231003

13   **Abstract:** The present study investigates the failure mechanisms of industrial fiber materials, using
14   a custom designed fiber cutting performance test bench. The fracture morphologies of single PA6
15   fibers are examined by scanning electron microscopy. The analysis reveals that fiber cutting can be
16   distinguished according to four distinct stages of fiber failure represented by shearing, cutting,
17   brittle fracture, and tensile failure, which are the result of different mechanisms active during the
18   processes of crack initiation, extension and fracture. The results of fractographic analysis are
19   further verified by an analysis of the blade assembly speed with respect to time over the entire
20   fracture failure process based on high-speed camera data. The results of fractographic analysis and
21   blade assembly speed are fully consistent.

22   **Keywords:** single fiber; cutting; fracture morphology; failure mechanism

23

24 1. Introduction

25   Natural and synthetic fibers can be employed to create materials with high strength, high elastic
26   modulus, light weight and low cost. Fibers play an irreplaceable role in many industries such as
27   national defense, aviation, aerospace and construction. The nature of fibrous materials make them
28   ideally suited to the manufacture of continuous sheets that must be subsequently cut into the
29   specific shapes required by industry, which consumes considerable energy. As such, considerable
30   effort has been expended to reduce the power consumption of the cutting process by way of
31   lowering cutting resistance based on the cutting mechanics of fibrous materials [1-4]. For example,
32   Dowgiallo [3] developed a rheological cutting energy model derived from experimental cutting tests
33   conducted for four different fibrous materials. Kakitis et al. [4] conducted experimental cutting tests
34   on six types of hemp fibers using a rotating knife. The researchers developed an interaction model
35   between the fiber and cutter, and proposed that the specific cutting energy depended on the extent
36   of rope twisting. In addition, fibrous materials are also commonly required to have extremely high
37   resistance to cutting and fracture failure. As a result, considerable effort has also been expended to
38   enhance the cutting resistance of fibrous materials [5-10]. For example, Kothari et al. [5] developed a
39   mathematical model for predicting the cutting resistance of woven cotton textiles. Vu Thi et al. [6]
40   studied the mechanics and mechanisms of cutting resistance for protective materials in the presence
41   of friction. Mayo and Wetzel [7] developed a model reflecting the static stress failure of fibers based
42   on experimental cutting resistance and failure results collected for six high-performance single fibers.
43   Kane et al. [8] studied the effects of impact force and rope tension on the cutting resistance of a
44   climbing rope cut with a handsaw.

The above summary indicates that considerable research has been conducted to evaluate the general forces involved with cutting resistance, and predictive models have been developed accordingly. However, we note that the cutting resistance of fibrous materials is generally based on the fracture mechanics of the individual fibers. Unfortunately, little work has been conducted from this perspective. The processes of crack initiation, extension, and fracture in individual fibers provide an accurate record of the conditions encountered during the cutting of fibrous materials. Therefore, qualitative analyses of the fracture mechanics of individual fibers will provide important evidence for developing fracture failure models and supply vital clues for diagnosing the causes of fracture failure and the mechanisms affecting cutting resistance.

To facilitate the above stated goals, this paper investigates the fracture mechanics of single PA6 fibers using a custom designed fiber cutting performance test bench. The fracture morphologies of the PA6 fibers are examined by scanning electron microscopy (SEM). Fractographic studies demonstrate the occurrence of different mechanisms active during the process of crack initiation, extension, and fracture. In addition, the fracture failure processes were recorded by high-speed camera, and a blade assembly speed variation curve is obtained. The analyses reveal four distinct fracture failure mechanisms active at different periods of the single fiber cutting process.

2. Materials and Methods

2.1. Test Materials

PA6 (polyamide, also known as nylon) is a fiber firstly developed by DuPont. PA6 is one of the most widely employed fibers in an extensive variety of applications, and presents good strength and mechanical performance. The testing conducted in this work employed single PA6 fibers (Nantong NTEC Monofilament Technology Co., Ltd.) 450 mm in length, 3 mm in diameter, with a density of 1.136×10^3 kg/m^3, tensile stress at fracture of 168 MPa, and a tensile deformation rate of 92.3%.

2.2. Test Bench

Figure 1 shows the custom-designed test bench employed for evaluation of fiber cutting. The bench mainly includes two clamping fixtures, cutting blade control and a test sensor system. The gauge length L_0 between the two clamping fixtures was 220 mm. The test system mainly includes an impact sensor installed on the top of the cutting blade and tensile stress sensors installed on the end of the clamping fixtures. The sensors can measure the forces acting on the fiber during cutting in real time. A high-speed camera was employed to record the cutting process at rate of 10,000 frames per second.
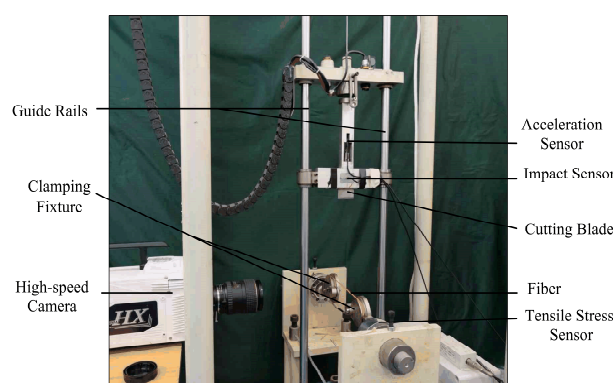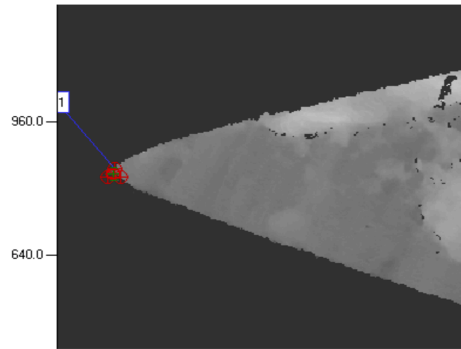

Figure 1. PA6 monofilament gravity cutting test bench

80
81   **Figure 2.** Representative optical micrograph of the blade tip showing an average edge radius of 15.1 ± 0.5 μm
82

83   The mass of the cutting blade assembly can be varied to evaluate its effect on cutting
84   performance, although only a single value of *m* was considered in the present work (2Kg). The
85   cutting blade consisted of high manganese steel with a blade tip angle of 30°. Figure 2 shows a
86   representative optical micrograph of the blade tip *r*. The cutting blade had an average tip radius *r* =
87   15.1 ± 0.5 μm based on measurements conducted using three similar images. Here, we note that the
88   sharpness of the blade increases with decreasing *r*. The cutting blade was positioned orthogonally
89   to the fiber during all tests.

90   *2.3. Test Process*

91   To mount a fiber for testing, one end of the fiber is clamped in the test fixture, and then the
92   fiber is pre-tensioned to 10% of its maximum tensile strength using a static weight attached to the
93   other end of the fiber. While under tension, the second fiber end is clamped in the test fixture. With
94   a single fiber mounted in the test fixture, the cutting blade assembly with a rest mass of m was
95   raised to a height h and released at zero initial speed. The cutting blade assembly then fell vertically
96   along the cylindrical guide rails under the force of gravity to cut the filament. The effect of friction
97   was reduced to a negligible concern by installing linear bearings between the cutting blade
98   assembly and guide rails. Therefore, friction in the apparatus was ignored during testing. Figure 3
99   illustrates the geometry of the cutting process for a 90° slice angle, where *h* is the initial distance
100   between the blade and fiber(which was preset in accordance with the requirements of the
101   experiment), *θ* is the angle of fiber deflection, *Δh* represents the vertical deflection of the fiber
102   (which equals the actual deflectionof the yarn's midpoint), which resolves the cutting force *F* into
103   tensile force *Ft* and compressive force *Fc* components.
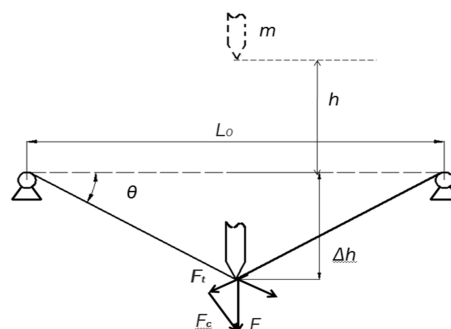

104
105   **Figure 3.** Conditions of fiber-blade contact at fiber failure with a 90° slice angle, showing a initial distance *h*, a
106   vertical deflection distance *Δh*, a fiber deflection angle *θ*, and tensile and compressive forces *Ft* and *Fc*,
107   respectively.

108   A major challenge when conducting cut testing is generating consistent, repeatable data. To
109   provide consistent data, ten samples were tested for each value of *m* and *h*. The characteristics of

110 fiber failure were examined by SEM using a JSM-5610LV (JEOL, Japan) field emission scanning
111 electron microscope with an accelerating voltage of 20 kV. To prepare fibers for SEM imaging, all
112 fibers (after failure) were sputtered with a few nanometers of silver using a JFC-1600 auto fine
113 coater (JEOL, Japan).

3. Results and Discussion

115 Based on the nature of the cutting apparatus employed, the cutting process can be divided into
116 three distinct stages: the initial stage, compression stage, fiber failure stage.

3.1. Initial Stage

118 Prior to contacting the fiber, the cutting blade assembly is in an approximate free fall condition.
119 When the blade initially contacts the fiber, the fiber is subject to an impact force, and axial elastic
120 stretching occurs. The fiber and blade assembly initially drop synchronously with negligible
121 interactive force between the two. Here, relative to the value of *m*, the mass of the fiber can be
122 ignored, and the blade assembly speed is not affected to a great extent in this stage.

3.2. Compression Stage

124 With increasing tension, the rate of axial elastic stretching decreases, producing an increasing
125 upward resistance force between the fiber and blade, which correspondingly reduces the blade
126 assembly speed. Conversely, the blade produces an increasing downward compressive radial stress
127 on the fiber. Under this condition, the fiber is subject to both increasing tensile stress and
128 compressive stress, which eventually reaches the fatigue limit of the fiber, whereupon the fiber
129 failure stage begins.

3.3. Fiber Failure Stage

131 As shown in Figure 4, a representative fractured fiber end presents four distinct fracture zones,
132 denoted as the craze-shearing zone, cutting zone, brittle-fracture zone, and tensile-failure zone, with
133 obvious borders between them. These areas reflect distinct fracture mechanisms associated with
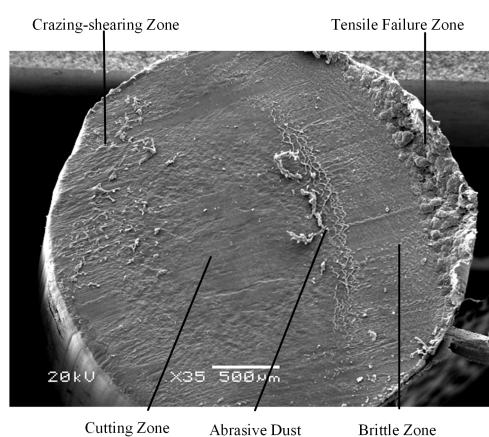134 crack initiation, crack extension, and fiber failure.

Figure 4.   SEM image of a representative fractured fiber end presenting four distinct fracture zones

3.1.1. Crack Initiation - Craze-shearing Zone

138 The action of the cutting blade on the fiber develops a local transverse compressive stress on the
139 fiber at the blade tip. For a fiber under tension, as in the present experimental configuration, this
140 transverse compression is likely to induce local flaws in the fiber such as cracks that then lead to

141 progressive local tensile failure. For a cutting blade acting with a force *F* at normal incidence on a
142 fiber of diameter *D*, the compressive stress induced by the blade σ_B is given approximately by

143 $\sigma_B = \dfrac{F_c}{2r\beta D}$, where *β* is a free adjustment factor. We assume *β*= 1 for the present study. In response to

144 increasing σ_B on the fiber and increasing fiber tension with the continued downward motion of the
145 blade assembly, the blade tip forms an indentation on the fiber surface owing to elastic deformation.
146 The depth of the indentation increases with increasing σ_B. Under this condition, the fiber on both
147 sides of the blade tip is stretched to the elastic limit, and plastic deformation occurs. Further increase
148 in σ_B gives rise to a large number of crazing and shearing belts within the fiber. This produces an
149 obvious shear yielding, while the fiber on both sides of the blade tip also undergoes craze yielding
150 due to increased tensile stress. This process induces the formation of cracks at the point of highest σ_B
151 under the blade tip.

152   Figure 5 presents a magnified SEM image of the craze-shearing zone shown in Figure 4. Here,
153 smooth fiber strands representative of craze fibrils are observed at the edge of the fiber fracture
154 surface. Plastic deformation of the craze fibrils is severe, and is accompanied with scattered fiber
155 fragments of various shapes and sizes. The fibrils in the craze-shearing zone are severely stretched
156 to a final length of about 100 μm, torn, and broken. The destruction is mainly caused by shear
157 yielding.

158
159   **Figure 5.**   SEM image of the craze-shearing zone shown in Fig. 4

160 3.3.2. Crack Extension - Cutting Zone

161   The compressive stress sustained by the fiber is perpendicular to the plane where the cracks
162 initially form. As the compressive and tensile stresses of the fiber increase, the blade travels through
163 the fiber along the initial cracks, forming a cutting section. At this point in the fracture process,
164 frictional forces act on the fiber in the same direction as that of crack extension. Thus, the fiber
165 material is stretched and undergoes plastic deformation due to friction.
166   Figure 6 presents a magnified SEM image of the cutting zone shown in Figure 4. We note that
167 the cutting cross section is relatively smooth, and the plastic deformation due to friction produces a
168 uniform distribution of stretched and broken features. We also note that the fibrils are stretched to a
169 final length of about 50 μm, the direction of plastic deformation is the same as that of crack extension,
170 and fiber fragments are sporadically scattered within the cutting zone.
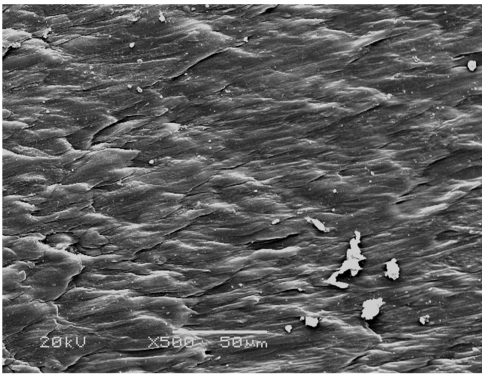171

172
173   **Figure 6.**   SEM image of the cutting zone shown in Fig. 4

174   3.3.3. Rapid Crack Extension - Brittle-fracture Zone

175   As the blade travels through the fiber, the effective cross-sectional area of the fiber decreases
176   while, simultaneously, the tension in the fiber increases due to the continued downward motion of
177   the cutting assembly. Eventually, the tensile stress exceeds the critical tensile stress of the fiber, and
178   cracks extend rapidly. At this point of the fracture process, the speed of crack extension is greater
179   than the speed of the cutting blade. Therefore, the blade is not in contact with the fiber, and zero
180   frictional force is applied to both sides of the cutting blade. Under the high frictional resistance in the
181   cutting zone, considerable debris accumulates on the cutting blade, which is then deposited on the
182   cutting face when fracture enters the rapid crack expansion stage. This explains the obvious line of
183   demarcation between the cutting zone and brittle-fracture zone observed in Figure 4.
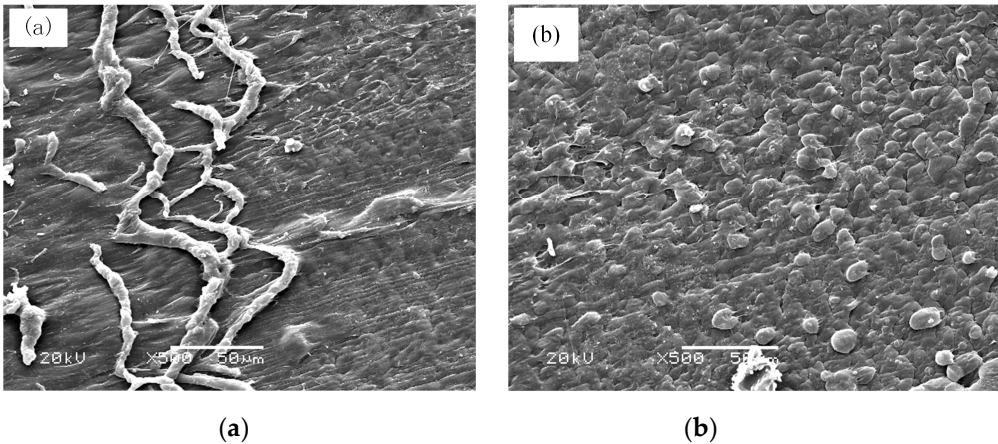

184

         (**a**)   (**b**)

185   **Figure 7.** SEM images of the area of abrasive dust accumulation (a) and brittle-fracture zone
186   (b) shown in Figure 4

187   Figure 7a and 7b respectively present magnified SEM images of the area of abrasive fiber dust
188   accumulation and the brittle-fracture zone shown in Figure 4. We note in Figure 7a that the debris
189   formed at the interface between the two cutting stages consists of twisted fiber material spread over
190   the cutting face. We note from Figure 7b that the brittle-fracture zone presents evenly distributed
191   fiber grains that are severed in the absence of plastic deformation. This verifies the absence of
192   frictional forces, indicating that cracks are extending at a greater speed than that of the blade
193   assembly.

194   3.3.4. Complete Failure – Tensile-failure Zone

195   With the occurrence of brittle fracture, the effective cross-sectional area of the fiber rapidly
196   reduces while fiber tension increases. The remaining cross-sectional area is overwhelmed by the
197   escalating level of fiber tension, and the fiber is completely and suddenly severed in a single

catastrophic event. Figure 8 presents a magnified SEM image of the tensile-failure zone shown in Figure 4. We note the formation of strands of fiber material that undergo rapid plastic deformation along the fiber axis prior to failure. The presence of very small tendrils of material indicates that some strands undergo extreme plastic deformation prior to failure. The uneven fracture surface presents no plastic deformation in the cutting direction.
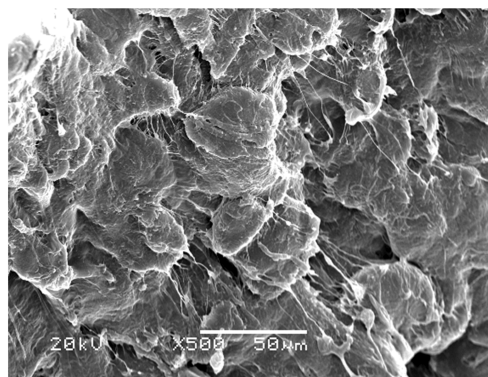

Figure 8.   SEM Image of the tensile-failure zone shown in Fig. 4

3.4. Blade Speed Variation during the Cutting Process

To objectively evaluate variations in the crack extension Speed, and to further demonstrate the fiber failure mechanism during fiber cutting, the blade assembly speed was determined from high-speed camera images, and the blade speed was plotted with respect to time over the entire cutting process beginning with the first contact between the cutting blade and the fiber.

As shown in Figure 9, the blade assembly speed fluctuates after first making contact with the fiber, indicating that the fiber initially vibrates prior to the compression stage. In the compression stage, the blade speed continues to fluctuate slightly. With increasing fiber tension, the blade assembly speed begins to decrease, and the fiber undergoes local compression under the normal force applied by the blade tip. The blade speed remains constant for a very short period until the value of   B exceeds that allowable by the fiber, whereupon the fiber undergoes plastic yielding, initial cracks are created, and the blade begins cutting into the fiber. The blade motion is then subjected to resistance owing to the frictional force between the fiber and the two sides of the blade. Hence, the blade speed decreases rapidly. The cutting resistance continues increasing while the effective cross-sectional area of the fiber rapidly decreases. The failure mechanism enters the brittle-fracture stage when the tensile stress reaches a critical value, and the crack extension speed begins to exceed the blade assembly speed, reducing the frictional force to zero. Hence, the blade assembly speed increases prior to complete fiber failure. The reduced friction and increased blade assembly speed has the effect of sweeping the debris from the blade surface onto the cutting face. After failure, the blade assembly speed naturally increases owing to an absence of resistance.

The foregoing analysis shows that the characteristic points on the blade assembly speed curve are fully consistent with the features of fiber fracture morphology obtained from SEM analysis. Future research will focus on the various parameters affecting the fracture failure mechanism, such as the effects of r, m, and h.
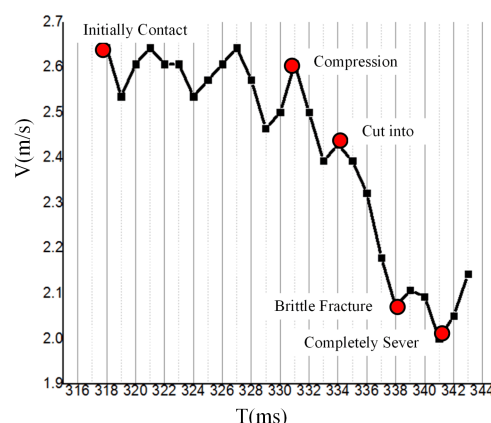
Figure 9. Blade assembly speed curve versus time over the entire cutting process

4. Conclusions

The present study investigated the failure mechanisms of long single PA6 fibers using a custom designed fiber cutting performance test bench. The fracture morphologies were examined by SEM. The analysis revealed that the fiber cutting process can be distinguished according to an initial stage, compression stage, and a fiber failure stage. The fiber failure stage was itself composed of four distinct stages represented by craze shearing, cutting, brittle fracture, and tensile failure, which are the result of different mechanisms active during the processes of crack initiation, extension and fracture. The fractographic analysis was further verified by an analysis of the blade assembly speed with respect to time over the entire fracture failure process based on high-speed camera data. The results of fractographic analysis and blade assembly speed were fully consistent. Craze shearing initially occurred owing to the development of a local transverse compressive stress on the fiber at the blade tip, wherein cracks were initiated. The blade assembly speed correspondingly decreased. During the cutting stage, the speed of crack extension was less than the speed of the blade assembly, and a substantial frictional force developed between the two sides of the cutting blade and the two fracture faces, resulting in extensive plastic deformation of the fracture face and a rapidly decreasing blade assembly speed. During the brittle-fracture stage, the speed of crack extension was greater than the speed of the blade assembly, resulting in a rapidly decreasing frictional force and increasing blade assembly speed. As a result, no plastic deformation was observed on the fracture face. Finally, tensile failure occurred when the remaining cross-sectional area was overwhelmed by the escalating level of fiber tension, and the fiber was completely and suddenly severed in a single catastrophic event.

Author Contributions: Zhitao He conceived and designed the experiments; Huiling Ding wrote the paper and performed the whole experiments; Yongzhen Zhang reviewed the manuscript.

Conflicts of Interest: The authors declare no conflict of interest.

References

1. Shin, H.-S.; Erlich, D. C.; Shockey, D. A. Test for Measuring Cut Resistance of Yarns. J. Mater. Sci. 2003, 38, 3603–3610.

2. Chen, Y.; Gratton, J. L.; Liu, J. Power Requirements of Hemp Cutting and Conditioning. Biosyst. Eng. 2004, 87, 417–424.

3. Dowgiallo, A. Cutting force of fibrous materials. J. Food Eng. 2005, 66, 57–61.

265   4.   Kakitis, A.; Berzins, U.; Berzins, R.; Brencis, R. Cutting properties of hemp fibre. In Cutting properties of
266   hemp fibre; Latvia University of Agriculture, Faculty of Engineering Jelgava: LUA, 2012; Vol. 24, pp.
267   245–250.
268   5.   Kothari, V. K.; Das, A.; Sreedevi, R. Cut resistance of textile fabrics---A theoretical and experimental
269   approach. Indian J. O F Fibre Text. Res. 2007, 32, 306–311.
270   6.   Vu Thi, B. N.; Vu-Khanh, T.; Lara, J. Mechanics and mechanism of cut resistance of protective materials.
271   Theor. Appl. Fract. Mech. 2009, 52, 7–13.
272   7.   Mayo, J.; Wetzel, E. Cut resistance and failure of high-performance single fibers. Text. Res. J. 2014, 84,
273   1233–1246.
274   8.   Kane, B.; Freilicher, M.; Cloyes, M.; Ryan, H. D. Impact Force and Rope Tension Affect Likelihood of
275   Cutting a Climbing Rope with a Handsaw. Arboric. Urban For. 2010, 36, 128–131.
276   9.   Ghahraei, O.; Ahmad, D.; Khalina, A.; Suryanto, H.; Othman, J. Cutting Tests of Kenaf Stems. Am. Soc.
277   Agric. Biol. Enginee 2011, 54, 51–56.
278   10.   Shin, H.-S.; Erlich, D. C.; Simons, J. W.; Shockey, D. A. Cut Resistance of High-strength Yarns. Text. Res. J.
279   2006, 76, 607–613.
280